OCO D-93260

OCO (Orbiting Carbon Observatory) - 2

Level 1B
Algorithm Theoretical Basis

Version 1.0 Rev 0
April 14, 2014

National Aeronautics and
Space Administration

JPL

Jet Propulsion Laboratory
California Institute of Technology
Pasadena, California

ORBITING CARBON OBSERVATORY (OCO) - 2

LEVEL 1B

Theoretical Basis Document

Annmarie Eldering	Jet Propulsion Laboratory
Randy Pollock	Jet Propulsion Laboratory
Richard Lee	Jet Propulsion Laboratory
Robert Rosenberg	Jet Propulsion Laboratory

Approved by:

Version 1.0
April 14, 2014

Jet Propulsion Laboratory
California Institute of Technology
Pasadena, California

Document History:

Version	Revision	Date	Description/Comments
1.0	0	April 14, 2014	Initial version of OCO-2 L1B ATBD

The research described in this document was carried out at the Jet Propulsion Laboratory,
California Institute of Technology, under a contract with the
National Aeronautics and Space Administration.

TABLE OF CONTENTS

1. Scope of This Document and Background

The OCO-2 Data User's Guide discusses the OCO-2 mission objectives and measurements, including instrument characteristics. Please refer to that document for details of the data collection and naming convention. The focus of this algorithm theoretical basis document (ATBD) is to describe the Level 1B data and the process used to transform the inherent instrument measurements (L1A data) into radiometrically calibrated spectra (L1B data, Figure 1). The reader is encouraged to obtain details of the analyses of the instrument test data from published articles referenced in this document.

1.1 Instrument Characteristics

The Observatory carries and points a single instrument that incorporates three co-boresighted, long-slit imaging grating spectrometers optimized for the O_2 A-band at 0.765 µm and the CO_2 bands at 1.61 and 2.06 µm (Figure 2) [Crisp et al. 2007; Crisp 2008]. The instrument mass is ~140 kg, and its average power consumption is ~100 Watts. The three spectrometers use similar optical designs and are integrated into a common structure to improve system rigidity and thermal stability. They share a common housing and a common F/1.8 Cassegrain telescope.

The light path is illustrated in Figure 2. Light entering the telescope is focused at a field stop and then collimated before entering a relay optics assembly. From there it is directed to one of the three spectrometers by a dichroic beam splitter and transmitted through a narrowband pre-disperser filter. The pre-disperser filter for each spectral range transmits light with wavelengths within ~±1% of the central wavelength of the CO_2 or O_2 band of interest and rejects the rest. The light is then refocused on the spectrometer slits by a reverse Newtonian telescope. Each spectrometer slit is ~3 mm long and ~25 µm wide. These long, narrow slits are aligned to produce co-boresighted fields of view that are ~0.0001 radians wide by ~0.0146 radians long.

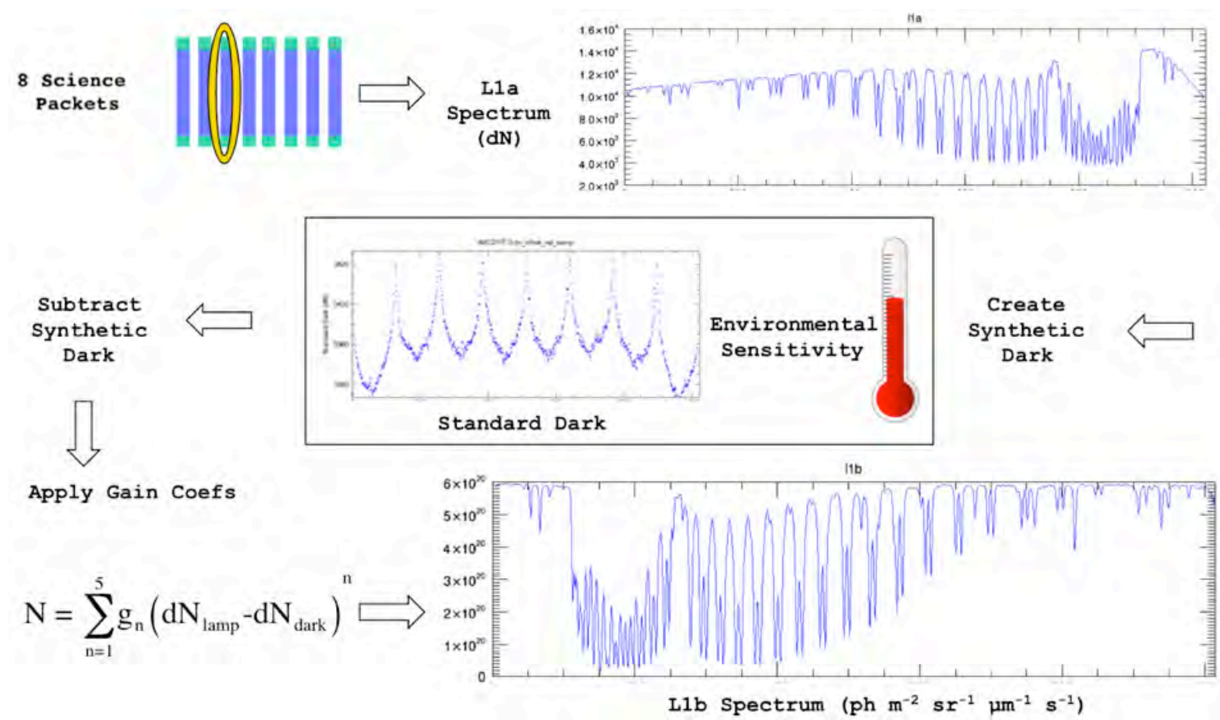

Figure 1. Overview of the ground processing data flow that results in L1B data.

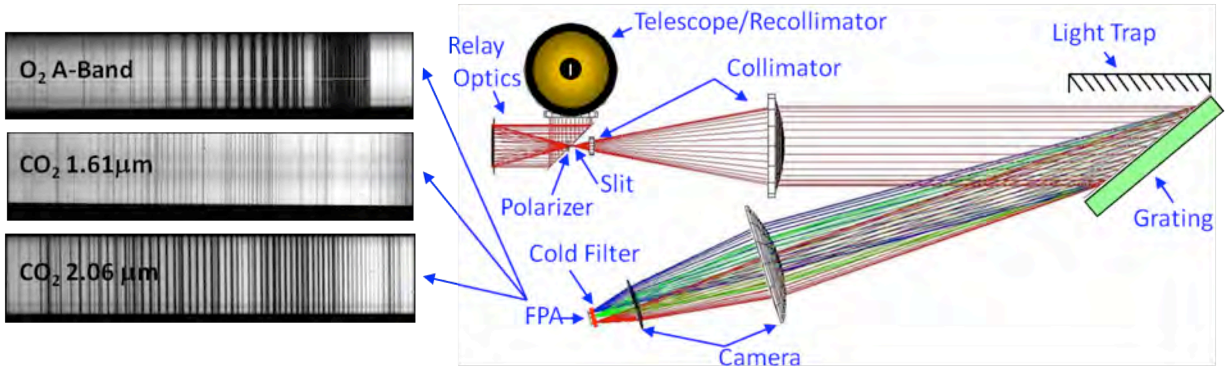

Figure 2. The OCO-2 instrument. (Left) Images of spectra recorded by the FPA in the three spectral channels. (Right) Major optical components and optical path.

Because the diffraction gratings efficiently disperse light that is polarized in the direction parallel to the slit, a polarizer is included in front of the slit to reject the unwanted polarization before it enters the spectrometer, where it could contribute to the scattered light background.

Once the light enters a spectrometer slit, it is collimated by a two-element refractive collimator, dispersed by a reflective planar holographic diffraction grating, and then focused by a two-element camera lens onto a two-dimensional focal plane array (FPA) after traversing a second narrowband filter. The narrowband filter just above the FPA is cooled to ~180 K to reject thermal emission from the instrument.

The spectral range and resolving power of each channel includes the complete molecular absorption band as well as some nearby continuum to provide constraints on the optical properties of the surface and aerosols, as well as absorbing gases. To meet these requirements, the O_2 A-band channel covers 0.758 to 0.772 μm with a resolving power of >17,000, while the weak 1.61 μm and strong 2.06 μm CO_2 channels cover 1.591 to 1.621 μm and 2.043 to 2.083 μm, respectively, with a resolving power in range of 18,000 to 20,000 [Crisp et al., 2007; Crisp 2008].

The gratings disperse the light onto the FPAs in the direction orthogonal to the long dimension of the slits (Figure 3). The field of view is resolved spatially along the slits. The FPAs are 1024 x 1024 pixel arrays with 18 μm by 18 μm pixels that have a 100% fill factor (i.e., there are no spatial or spectral gaps between the pixels). The slit is imaged on the FPA, which samples its full width at half maximum with two to three pixels.

The spectrum produced by each channel is dispersed to illuminate all 1024 pixels in spectral dimension on each FPA. The length of the slit limits spatial field of view to only ~190 pixels in the spatial dimension (Figure 3a). OCO-2 soundings use an along-slit field of view as defined by ~160 of these 190 pixels. In normal science operations, the FPAs are continuously read out at 3 Hz. To reduce the downlink data rate and increase the signal-to-noise ratio (SNR), 20 adjacent pixels in the FPA dimension parallel to the slit (i.e., the Spatial Direction in Figure 3a) are summed on board to produce up to eight spatially-averaged spectra (Figure 3b). The along-slit angular field of view of each of these spatially-averaged "super-pixels" is ~1.8 mrad (0.1° or ~1.3 km at nadir from a 705 km orbit). The angular width of the narrow dimension of the slit is only 0.14 mrad, but the telescope focus is purposely softened to increase the effective full-width at half-maximum of each slit to ~0.6 mrad to simplify the boresight alignment among the three spectrometer slits.

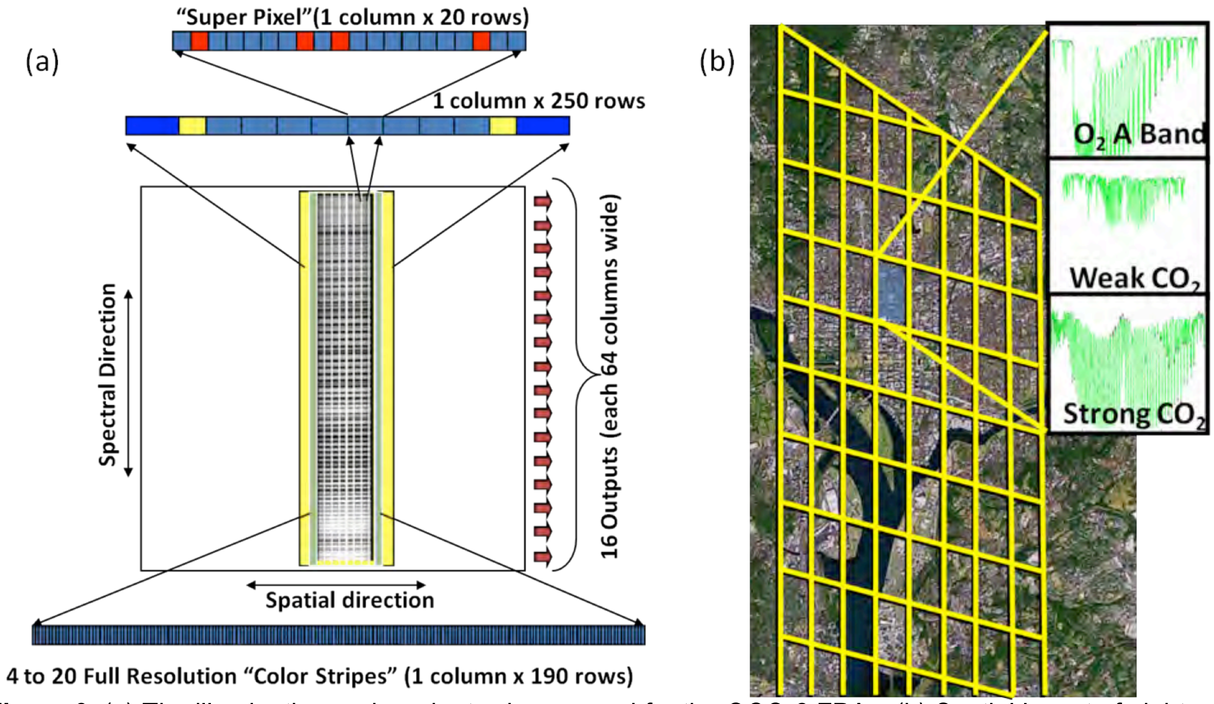

Figure 3. (a) The illumination and readout scheme used for the OCO-2 FPAs. (b) Spatial layout of eight cross-track footprints for nadir observations over Washington, D.C.

In addition to the eight spatially-binned, 1024-element spectra, each spectrometer also returns 20 spectral samples without on-board spatial binning to provide the full along-slit spatial resolution. Each of these full-resolution "color stripes" covers a 220-pixel-wide region of the FPA that includes the full length of the slit (190 pixels) as well as a few pixels beyond the ends of the slit (Figure 3a). These full-spatial-resolution color stripes are used to detect spatial variability within each of the spatially-summed super-pixels and to monitor the thermal emission and scattered light within the instrument.

Note that for science analysis, only 1016 of the 1024 spectral elements are carried in the L1B file (four reference pixels on two sides of the array are excluded). The L2 dataset may include fewer than 1016 of the 1024 elements, as focal plane samples that are too noisy are eliminated from the L2 data analysis.

1.2 Radiometric Overview

The focal planes are read out in unitless data numbers (dNs), and these are referred to as the L1A Spectrum (see Figure 1). The first data processing step is to apply dark correction. During thermal vacuum testing, a set of data was collected with the light source shuttered such that no light entered the instrument. This dark data is used to characterize the response of the focal planes with no illumination. As discussed in Rosenberg et al. [2014], this is important because a dN offset can introduce a linearity error. During orbit, dark data will be collected and the dark subtraction will be updated early in the mission. The dark data will be monitored thereafter and updated if needed.

The next step is to apply gain curves, which describe the relationship between dN and calibrated radiance. The preflight gain curves are described in more detail in Rosenberg et al. [2014]. The sections below describe the approach for in-flight updates.

1.3 Spectral Response Overview

To properly use the L1B data, the instrument line shapes (ILS) must be determined. These are contained in the L1BSc files in two key fields: ils_delta_lambda and ils_relative_response. ILS are covered in more detail below, and their use is described in the Data User's Guide.

Dispersion coefficients are also provided in the L1BSc files (dispersion_coef_samp) to convert the focal plane sample pixel index to a wavelength scale. In the L2 retrieval of geophysical quantities, the Doppler shift is accounted for and the dispersion is corrected for each sounding.

1.4 In-Flight Measurements

In flight, three radiometric calibration measurements are routinely collected: solar calibration, dark calibration, and vicarious calibration data.

For solar calibration, the Observatory views the Sun through the diffuser just before eclipse, holding a steady viewing angle to observe atmospheric spectra at various optical depths unaffected by significant pressure broadening or surface reflection. These measurements are used to verify the spectral response of the spectrometer.

For dark calibration, the Observatory collects data with the aperture door closed and the lamps off (Figure 4). This calibration is repeated at various eclipse-side latitudes.

For vicarious calibration, the Observatory targets Railroad Valley, Nevada, a ground site with a well-characterized surface, where there is sufficient instrumentation to make absolute radiance measurements. More details can be found in Kuze et al. [2011; 2013].

2. Radiometry

2.1 Dark Subtraction

Temperature variations of the optics and FPAs contribute to the dark background signal. The as-measured dN values can be corrected for these effects using the dark subtraction equation:

$$dn_{corrected} = \left(dn_{raw} - dn_{ref}\right) + c_{optics}(T_{optics}(t) - T_{ref\_optics}) + c_{FPA}(T_{FPA}(t) - T_{ref\_FPA})$$

where

- $dn_{corrected}$ —dN after dark correction
- dn_{raw} —as-measured dN
- dn_{ref} —dN detected with no illumination
- c_{optics} —optics temperature dependence coefficients
- T_{optics}(t) —optics temperature as a function of time (in L1B data product as FrameTemperatures/temp_smooth_optical_bench_grating_mz)
- T_{ref_optics} —the optics temperature that will yield dn_{ref}
- c_{FPA} —FPA temperature dependence coefficients
- T_{FPA}(t) —O_2, weak CO_2, and strong CO_2 FPA temperatures as a function of time (in L1B data product as FrameTemperatures/temp_smooth_fpa_[o2, weak_co2, strong_co2])
- T_{ref_FPA} —the O_2, weak CO_2, and strong CO_2 FPA temperatures that will yield dn_{ref}

dn_{raw}, dn_{ref}, c_{optics}, and c_{FPA} have dimensions of 1024 x 8 x 3—a value for each column, footprint, and band. These are in the Ancillary Radiometric Product (ARP) but are not provided in the L1B files.

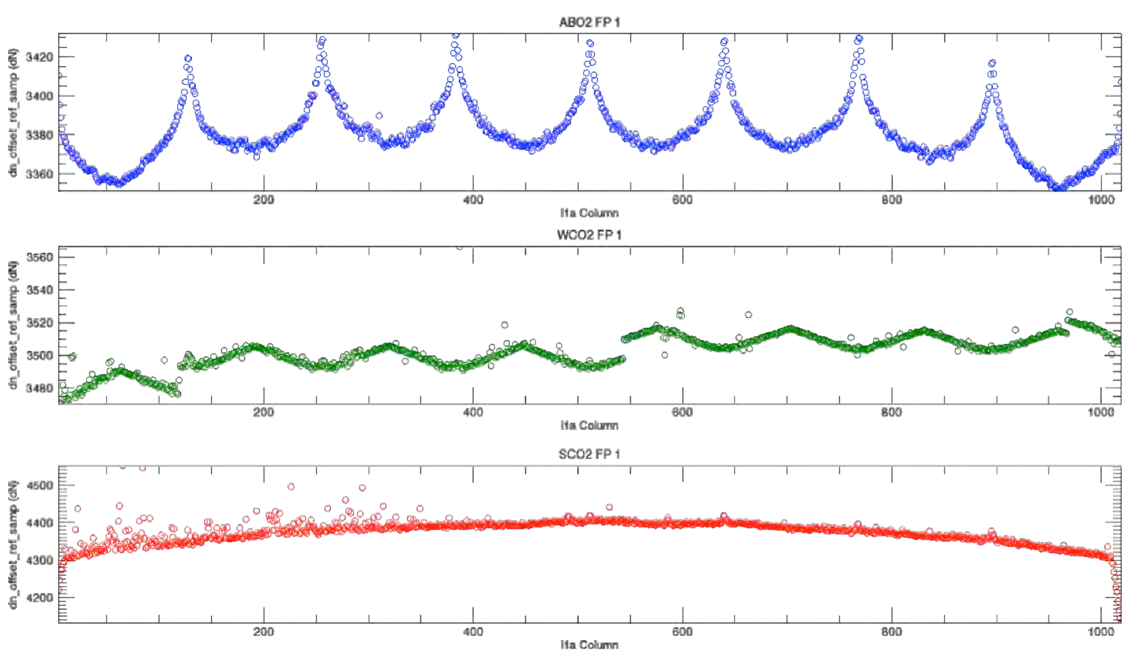

Figure 4. Example of a term in the dark subtraction (dn_{raw}).

The pre-launch ground testing provides the initial set of coefficients for these terms. The strongest sensitivity by far is that of the strong CO_2 signal to the optical bench temperature. On the original Orbiting Carbon Observatory, a weaker connection was found between the O_2A-band signal and focal plane temperature, but on OCO-2 this was found to be insignificant because the detector is cooled to 120 K as opposed to 180 K. No significant connection was observed for the weak CO_2 signal except a local sensitivity to focal plane temperature in the proximity of bad pixels that extend charge across entire rows.

For initial data processing after launch, the reference dark will be based on data from the final ground-based instrument thermal vacuum testing. The temperature coefficients will be set to zero initially and updated once there are on-orbit measurements.

2.2 Radiometric Gain

Because atmospheric absorption is inferred from the ratio between continuum and line core radiances, the radiometric calibration must account for any nonlinearities in the instrument gain. Even though the instrument gain appears near linear, it is described using a 5th order polynomial of radiance vs. signal to describe any nonlinear effects:

$$Radiance = k\sum_{i=0}^{5} c_i\left(dn_{dark\_corrected}\right)^i$$

The k terms, referred to as gain_degrad_samp, (k) will be set to 1.0 at launch. The gain_degrad_samp term in-flight will be determined through the vicarious calibration experiments that were mentioned earlier.

The c_i terms are referred to as gain_preflight_samp, (c_i). At launch, these are set based on a combination of the best five radiometric calibration tests during final instrument testing at JPL. While the algorithm allows an offset term ($i = 0$), the c_0s are all set to zero as dark subtraction is made in the earlier computational step. No significant improvement was observed after cubic correction, so the c_4s and c_5s are also set to zero. The determination of the gain_preflight_samp coefficients is described in detail in Rosenberg et al. [2014]. These values will not change on-orbit except in samples with newly-flagged bad pixels.

An example of the application of this equation (for the strong CO_2 band, column 500, footprint 3) is:

$$\text{Radiance} = 0 + 2.898 \text{ x } 10^{15} \cdot \text{dn} + 1.902 \text{ x } 10^{9} \cdot \text{dn}^2 + 9.559 \text{ x } 10^{3} \cdot \text{dn}^3 + 0 \cdot \text{dn}^4 + 0 \cdot \text{dn}^5$$

3. Signal-to-Noise Ratio

3.1 Calculation of SNR

The noise values are not stored directly in the file, but they can be calculated using a few fields in the L1bSc data file and the following formulas for the noise equivalent radiance and consequently the SNR:

$$NEN = \frac{MaxMS}{100} \cdot \sqrt{\left|\frac{100 \cdot N}{MaxMS}\right| \cdot C_{photon}^2 + C_{background}^2}$$

$$SNR = \sqrt{\frac{100\ N^2}{MaxMS * (C_{background}^2 \frac{MaxMS}{100} + C_{photon}^2 N)}}$$

where

- N —radiance value
- $MaxMS$ —maximum measurable signal per band (see below)
- C_{photon} —first coefficient of L1bSc/InstrumentHeader/snr_coef ([0, *, *, *])
- $C_{background}$ —second coefficient of L1bSc/InstrumentHeader/snr_coef ([1, *, *, *])

The third entry of L1bSc/InstrumentHeader/snr_coef (zero-based indices [2, *, *, *]) is used to identify bad samples that should be excluded by the retrieval algorithms. The third entry will be 1 if the sample is bad and 0 if it is good. Figure 5 shows an example set of coefficients.

The *MaxMS* values are given in Table 1 below. The strong CO2 value was increased by 50% from OCO, and all values were halved to account for only one polarization being selected.

Table 1. *MaxMS* values.

Band	MaxMS value (photons/m^2/sr/µm)
O_2 A-band	$7.00*10^{20}$
Weak CO_2	$2.45*10^{20}$
Strong CO_2	$1.25*10^{20}$

3.2 Development of SNR Coefficients

The initial snr_coef are based on a combination of the data from the best five radiometric calibration tests during final instrument testing at JPL. While this model assumes a perfectly linear detector, which is not the case, it still fits the data reasonably well. The only significant errors observed are at extremely low signal levels, where this SNR expression overestimates the radiance uncertainty because we do not currently include a term for uncertainty due to dark subtraction. The importance of this term will be further investigated in flight.

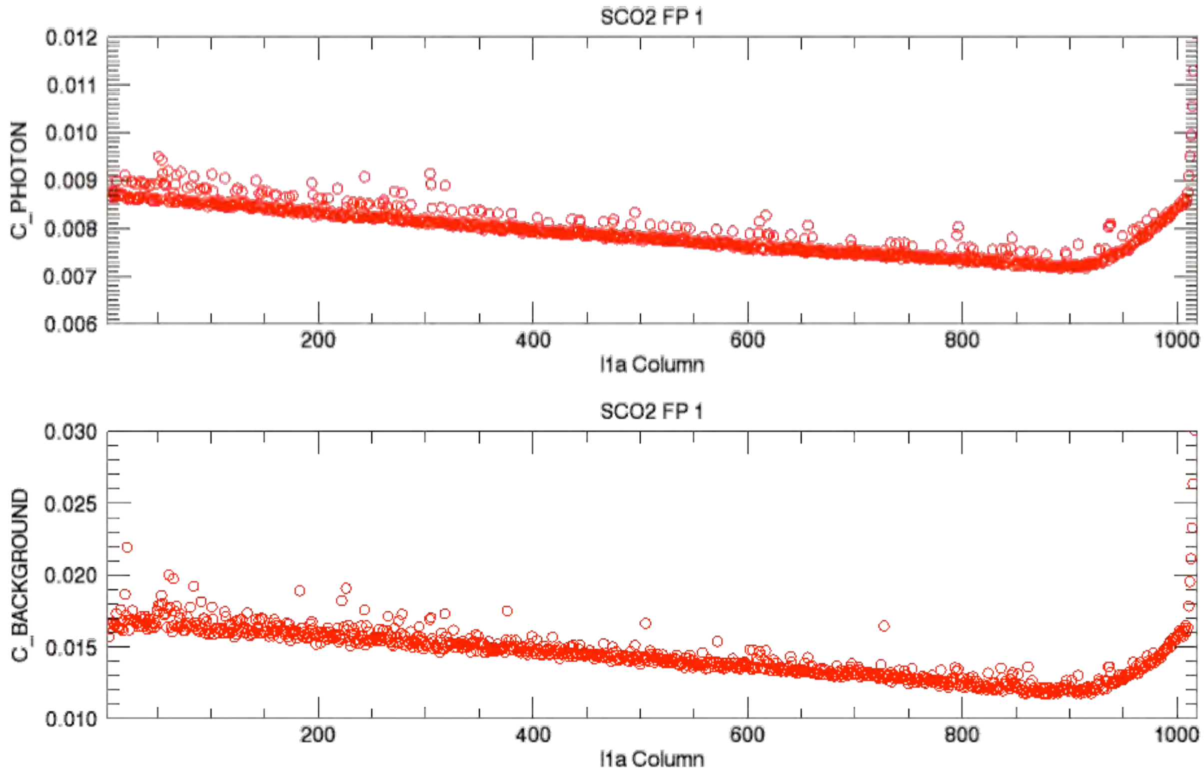

Figure 5. Example of signal-to-noise coefficients.

3.3 In-Flight Updates of SNR Coefficients

The dark noise (background term) will be updated based on the dark calibration data, measured directly during dark calibration periods (~12 two-minute dark calibration data collections each day).

Photon noise is assessed using solar calibration and lamp calibration data (our only consistent radiance scenes). We assume that the photon noise changes if the gain_degrad_samp term changes and adjust accordingly.

Later in the mission, a further assessment of the photon noise will be conducted by analyzing any changes in the residuals (differences between observed and calculated spectra determined in the L2 retrieval stage) for scenes that appear to have consistent radiances and retrieved state.

4. Spectral Response

4.1 Spectral Dispersion Coefficients

The dispersion coefficients express the relationship between the spectral element index (an individual pixel) and its associated wavelength (see Figure 6). These data are contained in L1bSc/InstrumentHeader/dispersion_coef_samp. Note that this grid does not account for the Doppler correction or dispersion adjustments that are applied in the L2 retrieval stage. The coefficients are used as follows:

$$\lambda = \sum_{i=0}^{5} c_i \ . \ \mathrm{column}^i$$

where column refers to the column number in the L1bSc files (1 to 1016), which is raised to the power i.

An example calculation of the wavelength grid is:

$$\begin{aligned}\lambda = &\ 0.757633 + 1.75265 \times 10^{-5} \cdot \mathrm{column}^1 \\ &- 2.91788 \times 10^{-9} \cdot \mathrm{column}^2 + 3.29430 \times 10^{-13} \cdot \mathrm{column}^3 \\ &- 2.72386 \times 10^{-16} \cdot \mathrm{column}^4 + 7.66707 \times 10^{-20} \cdot \mathrm{column}^5\end{aligned}$$

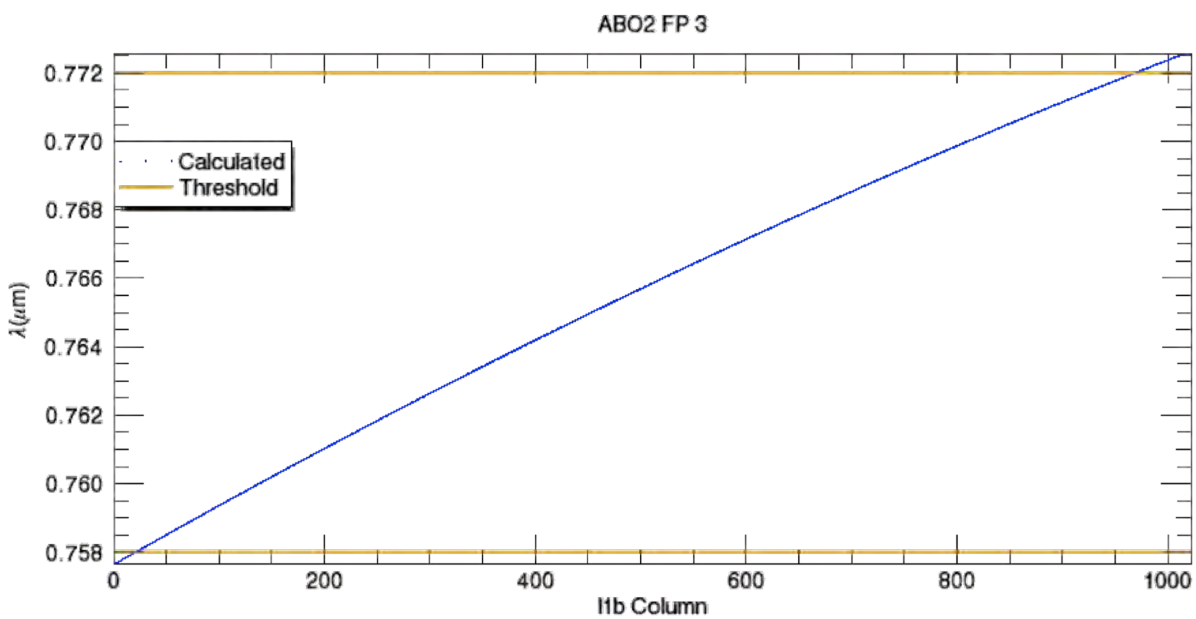

Figure 6. An example of the conversion of the focal plane column to wavelength scale. The blue line shows the column number-to-wavelength transformation. The yellow lines indicate the required wavelength range for this band.

4.2 Instrument Line Shape

The central challenge of the OCO-2 spectral calibration is determining not just a single ILS, but rather the ILS for each and every spectral pixel index, footprint, and band. The three bands, eight footprints per band, and 1016 spectral samples per footprint yield in theory 24,384 individual ILS functions. This is in contrast to, e.g., the Thermal and Near Infrared Sensor for Carbon Observations-Fourier transform spectrometer (FTS) aboard the Greenhouse Gases Observing Satellite (GOSAT), which in theory has just two ILS functions (one per polarization), as described by Yoshida et al. [2012]. However, the physics of the OCO-2 instrument design dictates that the ILS and centroid wavelength response (dispersion) of OCO-2 should vary smoothly in the spectral dimension across each band. The details of the measurements and analysis for determining the ILS are reported in Lee et al. [2014].

In the data product, for each band, footprint, and spectral element (3 x 8 x 1016 pixels), there are two 200-element lookup tables: L1bSc/InstrumentHeader/ils_delta_lambda and L1bSc/InstrumentHeader/ils_relative_response.

Initial determination of the ILS was performed using tunable diode lasers that were stepped through a range of wavelengths covering the OCO-2 spectral range. The final ILS was then optimized and validated by comparing solar spectra recorded simultaneously by OCO-2 and an FTS, as described by O'Dell et al. [2011]. As reported in Lee et al. [2014], the resulting ILS profiles (Figure 7) showed agreement between the two spectra to approximately 0.2% rms, satisfying the preflight calibration requirement of < 0.25% rms.

At the start of the mission, ils_delta_lambda and ils_relative_response are based on several laser and heliostat-based tests at JPL. Early mission spectral residuals will be carefully examined to evaluate the representativeness and accuracy of the preflight ILS.

Spectral residuals created during the retrieval stage using on-orbit data will be carefully analyzed for evidence of ILS errors. In the long term, the solar calibration mode provides an opportunity to look at relative changes in the ILS due to Doppler shifts. However, since the flight diffuser may make subtle changes the ILS, an absolute measurement may not be possible.

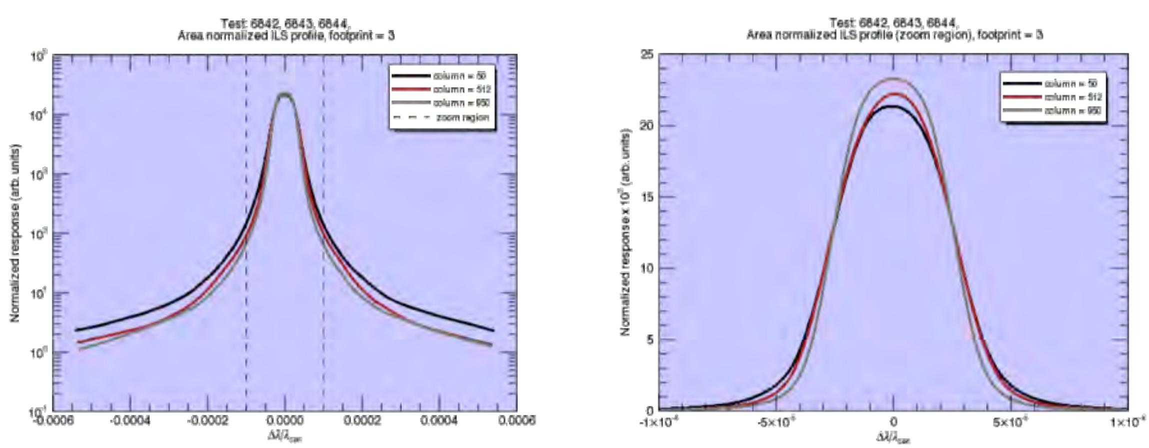

Figure 7. Example ILS profiles for the O_2 A-band at three different spectral pixel indexes. (Left) Semi-log plot of the ILS.(Right)Linear plot of the ILS core.

5. Ancillary Radiometric Product Files

The key calibration parameters are stored in the ARP, which is not distributed publically. These files are changed as needed and deemed necessary. Prior to launch, this is expected to be weekly. There will be an ARP file for initial processing and an updated ARP for reprocessing to reflect any additional knowledge gained from the measured data set about temperature dependence, dark subtraction, etc. Each of the data products identifies the ARP used in Metadata/ARPAncillaryDatasetDescriptor.

6. Other Resources

There are a number of other project documents that the user should refer to as they work with the data.

1. Data User's Guide—This document discussed the publically distributed data products, L1bSc, L2IDP, L2Std, and L2Dia. The key data fields are discussed, and tables are included that specify all of the fields in each data product.
2. L2 ATBD—This ATBD steps through the physics and implementation of the Level 2 algorithm.
3. ATBD for IMAP-DOAS and ABO2—These ATBDs describe the two methods of identifying potentially cloudy footprints, in what we refer to as the prescreening step. These data are then used for setting data quality and data selection levels.
4. Published papers—There are a number of published papers describing the algorithm, application to GOSAT, prescreening steps, etc. Please see the most up-to-date list of publications on oco2.jpl.nasa.gov

7. References

Crisp, D., C. E. Miller, and P. L. DeCola, NASA Orbiting Carbon Observatory: Measuring the column averaged carbon dioxide mole fraction from space, *JARS*, (2007).

Crisp, D., The Orbiting Carbon Observatory: NASA's First Dedicated Carbon Dioxide Mission, *Proc. SPIE,* 7106 (2008). doi: 10.1117/12.802194.

Kuze, Akihiko, et al. Long-Term Vicarious Calibration of GOSAT Short-Wave Sensors: Techniques for Error Reduction and New Estimates of Radiometric Degradation Factors. *IEEE Transactions on Geoscience and Remote Sensing,* 52.7 (2013): 1-14.

Kuze, Akihiko, et al. Vicarious calibration of the GOSAT sensors using the Railroad Valley desert playa. *IEEE Transactions on Geoscience and Remote Sensing*, 49.5 (2011): 1781-1795.

Lee et al., Preflight Spectral Calibration of the Orbiting Carbon Observatory-2, in preparation, 2014.

O'Dell, C. W., J. O. Day, R. Pollock, C. J. Bruegge, D. M. O'Brien, R. Castano, I. Tkatcheva, C. E. Miller, and D. Crisp, Preflight Radiometric Calibration of the Orbiting Carbon Observatory *IEEE Transactions on Geoscience and Remote Sensing*, 49.6 (2011): 2438-2447.
doi: http://dx.doi.org/10.1109/TGRS.2010.2090887.

Rosenberg et al., Preflight Radiometric Calibration of Orbiting Carbon Observatory 2, in preparation, 2014.

Yoshida, Y., N. Kikuchi, and T. Yokota. On-orbit radiometric calibration of SWIR bands of TANSO-FTS onboard GOSAT. *Atmospheric Measurement Techniques Discussions*, 5.4 (2012): 4711-4734.